Applied Thermal Engineering 213 (2022) 118664

Contents lists available at ScienceDirect

Applied Thermal Engineering

journal homepage: www.elsevier.com/locate/apthermeng

Research Paper

A study on the upper limit efficiency of solar still by optimizing the mass transfer

Guilong Peng, Zhenwei Xu, Jiajun Ji, Senshan Sun, Nuo Yang *

State Key Laboratory of Coal Combustion, School of Energy and Power Engineering, Huazhong University of Science and Technology, Wuhan 430074, China

ARTICLE INFO

Keywords:
Solar still
Desalination
Heat and mass transfer
Upper limit
Air circulation

ABSTRACT

Solar still is an green energy, low-cost and easy-to-maintain desalination system. Enhancing the mass transfer is a very important strategy for improving solar still. However, the analysis of the upper limit performance of the solar still related to the optimized mass transfer is lacking. In this work, by assuming the most ideal heat and mass transfer condition in solar still, the theoretical upper limit performance of solar still is given. The theoretical results reveal that the mass transfer in solar still is sensitive to the inner air circulation. The mass transfer in the solar still reaches up to the upper limit quickly when the air circulation is enhanced. By enhancing the mass transfer process, the theoretical upper limit of the energy efficiency in solar still is around 87%, 91.5%, and 94.5%, respectively, for the input power density at 300 W/m^2, 500 W/m^2, and 700 W/m^2. Experimental results show that in a solar still with the basin size at 25 cm × 25 cm, the theoretical upper limits can be approached by only using 0.2 W ~ 0.6 W of fan power. Compared to the efficiency of conventional solar still without modification, the upper limit energy efficiency is 48%, 28%, and 20% higher, respectively, under 300 W/m^2, 500 W/m^2, and 700 W/m^2 input power density. Meanwhile, to reach the upper limit, the total extra cost of the modification can be as low as 3 $ by using a fan in solar still. This work offers a new understanding of the mass transfer process and provides an effective and economical optimizing way not only for the solar still but other themal systems with heat and mass transfer.

1. Introduction

The demand for freshwater has increased dramatically in the last decades due to the development of agriculture and industry, as well as the growth of population [1]. It is reported that billions of people are suffering from freshwater scarcity [2]. Given the abundance of seawater, it is promising to obtain freshwater by desalination [3]. Solar desalination is a popular and eco-friendly desalination technology that draws much attention in both industry and academic fields [4,5]. Solar stills (SSs) are the most widely used desalination systems that are especially suitable for off-grid freshwater supply in remote areas, islands, ships, and so on. Nevertheless, the energy efficiency of the conventional SSs are usually around 30% and have ample room for further modifications [6–8].

In general, the modifications can be classified into two kinds of strategies: (1) enhancing the solar absorption; (2) enhancing the mass transfer. In the aspect of solar absorption, many new materials with high absorptivity have been developed recently, such as hydrogel [9,10], graphene aerogel[11,12], porous metallic materials[13,14] etc. Regardless of the inherent reflectance of the glass cover, the solar absorption in SSs can be improved to near the upper limit (>99%) by using nano/micro porous materials or coatings [5,15].

On the other hand, to improve the mass transfer, much attention has been paid to enhancing the temperature difference between the evaporation and condensation surface in various SSs, such as using film cooling [16,17], thermal-electrical cooling [18,19], external condenser [20–22], heat localization on the evaporation surface [23,24], heat exchanger [25], and so on, as well as the combination of them. These modifications either enhance the water temperature or decrease the glass temperature, or both, hence higher mass concentration gradient and better mass transfer performance in SSs.

However, the upper limit performance of solar still by taking full advantage of the mass transfer in SSs are less studied and discussed, let alone strategies to achieve it efficiently and economically. The knowledge of the upper limit is of significant importance to the design, analysis, and comparison of different modifications. Conventional theories use empirical correlations as well as heat and mass transfer analogy and fail to predict the upper limit [26–28]. Therefore, it is necessary and urgent to analyze the mass transfer from a new point of view.

* Corresponding author.
E-mail address: nuo@hust.edu.cn (N. Yang).

https://doi.org/10.1016/j.applthermaleng.2022.118664
Received 20 August 2021; Received in revised form 11 March 2022; Accepted 14 May 2022
Available online 20 May 2022

Nomenclature

Cp_{mix}	Specific heat capacity of the saturated moist air [J/(kg·K)]
Cp_w	Specific heat capacity of the water [J/(kg·K)]
d	Moisture content of the air [kg/kg]
h_a	Convective heat transfer coefficient between the glass cover and the ambient [W/(m^2·K)]
h_{h2}	Convective heat transfer coefficient of the air circulation [W/(m^2·K)]
h_{m2}	Convective mass transfer coefficient of the air circulation [m/s]
h_{fg}	Latent heat of the vapor [J/kg]
h_{LV}	Total enthalpy of phase change [J/kg]
I	Input power density [W/m^2]
$\dot{m}_a$	Mass flow rate of the dry air [kg/(m^2·s)]
$\dot{m}_{mix}$	Mass flow rate of the moist air [kg/(m^2·s)]
$\dot{m}_v$	Productivity of the solar still [kg/(m^2·s)]
P	Total pressure of the air [Pa]
P_f	Vapor pressure of the air flow[Pa]
P_F	Power of the fan [W]
P_g	Vapor pressure at T_g [Pa]
P_v	Vapor pressure [Pa]
P_w	Vapor pressure at T_w [Pa]
$q_{c(g\_a)}$	Heat convection flow between the glass cover and the ambient [J/m^2]
$q_{c(w\_g)}$	Heat convection flow between the water and the glass cover [J/m^2]
$q_{d(b\_a)}$	Heat conduction flow between the ambient and the basin [J/m^2]
$q_{e(w\_g)}$	Heat flow of phase change [J/m^2]
$q_{r(g\_a)}$	Heat radiation flow between the glass cover and the ambient [J/m^2]
$q_{r(w\_g)}$	Heat radiation flow between the water and the glass cover [J/m^2]
$R_{g,v}$	Gas constant of the vapor [J/(kg·K)]
$R_{g,a}$	Gas constant of the dry air [J/(kg·K)]
SS	Solar still
T_{amb}	Ambient temperature [K]
T_g	Temperature of the glass cover [K]
T_{f1}	Temperature of the up-flow moist air [K]
T_{f2}	Temperature of the down-flow moist air [K]
T_w	Temperature of the water [K]
V	Air circulation velocity [m/s]

Greek letters

γ	The ratio between the surface area of the glass cover and the water
ε_1	Emissivity between the water and the glass cover
ε_2	Emissivity between the glass cover and the ambient
ε_w	Emissivity of the water
ε_g	Emissivity of the glass cover
η_s	Energy efficiency of solar still [%]
ρ_v	Density of the vapor [kg/m^3]
ρ_{mix}	Density of the moist air [kg/m^3]
σ	Stefan-Boltzmann constant [W/(m^2 Â· K^4)]
∅	Relative humidity [%]

In this work, by assuming the most ideal mass transfer condition in solar still, the theoretical upper limit performance of solar still is given, and also approached in experiments. Firstly, the theoretical model is proposed based on the conservation of both heat and mass. Then, it is studied theoretically the effects of the input power density, inner air circulation, ambient air convection, as well as ambient temperature. Based on the analyses, the theoretical upper limit of the energy efficiency of mass transfer is obtained. Lastly, the experiments are carried out and the measured results are compared with the theoretical predictions.

2. Methods

2.1. Theoretical model

Fig. 1a shows a typical SS consisting of six main parts, including the basin, seawater, glass cover, insulation, grooves, and bottles. The basin absorbs most of the solar irradiation and heats the seawater above it. The water evaporates and flows up to the glass cover. The temperature of the glass cover is lower than that of water vapor, thus the vapor condenses as droplets on the glass cover. Later, the droplets grow up and finally flow down as freshwater to the grooves that are connected with a bottle. The high concentration brine will be rejected to another bottle. To decrease the heat loss, the insulation material is used on the basin and walls.

The main heat transfer process of SS is shown in Fig. 1b. The absorbed energy in the basin is either transported to the water above it or dissipated to the ambient. The energy in the water is transported to the glass cover by the air convection $q_{c(w\_g)}$, radiation $q_{r(w\_g)}$, and phase change processes $q_{e(w\_g)}$. The glass cover dissipates the heat to the ambient via heat convection $q_{c(g\_a)}$ and radiation $q_{r(g\_a)}$. The energy efficiency of mass transfer can be obtained by analyzing the conservation of heat and mass transfer between ambient, basin, water, and glass cover.

Herein, to investigate the upper limit of efficiency, an ideal model is proposed by making the following assumptions:

a) The air is heated to the water temperature T_w before leaving the water–air interface, and is cooled down to the glass temperature T_g before leaving the air-glass interface (Fig. 1c), i.e.,

$$T_{f1} = T_w \tag{1}$$

$$T_{f2} = T_g \tag{2}$$

b) The air temperature remains constant and the air saturated, after leaving the water–air interface and before reaching the air-glass interface (Fig. 1d).

c) The temperature as well as the heat and mass transfer rates are uniform at the interfaces.

d) The heat loss from the basin to the ambient is zero.

e) The airflow velocity profile is uniform and centrosymmetric in the SS.

Based on the conservation of energy, it can be obtained that,

$$I = q_{r(w\_g)} + q_{d(b\_a)} + q_{e(w\_g)} + q_{c(w\_g)} \tag{3}$$

where I is the input power density, corresponding to the absorbed solar energy in practical applications. $q_{r(w\_g)}$, $q_{e(w\_g)}$, $q_{c(w\_g)}$ are the heat flows from the water to the glass cover by radiation, phase change, and convection, respectively. $q_{d(b\_a)}$ is the heat flow from the basin to the insulation and ambient by heat conduction, which is regarded as zero in the ideal model. The overall energy efficiency, η_s, is defined as the ratio of the phase change enthalpy to the total input power[26],

$$\eta_s = \frac{q_{e(w\_g)}}{I + P_F} \times 100\% \tag{4}$$

where P_F is the power density that is used to enhance the inner air circulation. In the ideal situation, the relationship between P_F and the

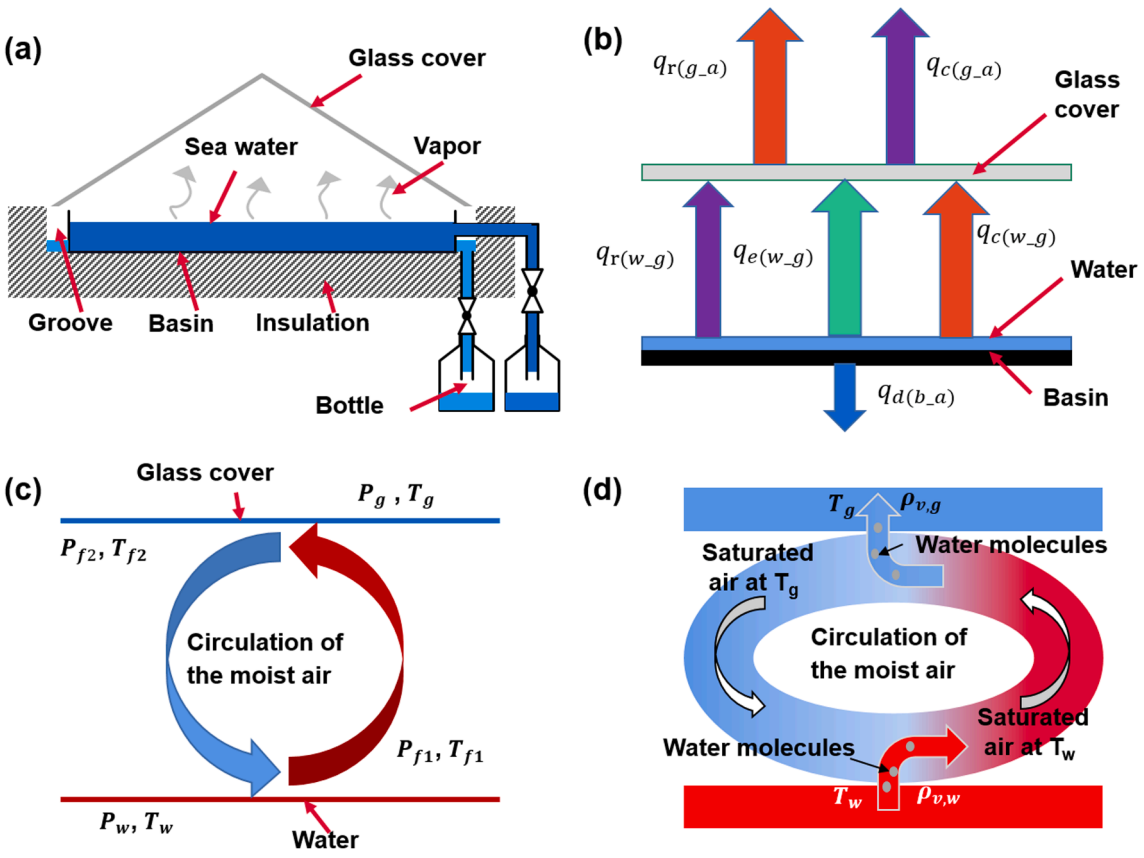

Fig. 1. Theoretical model of the SS. (a) The schematic diagram of a typical SS. (b) The heat transfer process in SS. (c) Model of the ideal convective air circulation in SS. (d) Ideal humidification and dehumidification process in SS.

enhanced air circulation velocity V can be descript as[29]:

$$P_F = \frac{1}{2}\rho_{mix} V^3 \tag{5}$$

In SS, the mass transfer is mainly driven by air circulation as shown in Fig. 1c. The air is heated and humidified near the water surface to be saturated at temperature T_{f1}, and vapor pressure P_{f1}. Then the moist air is cooled and dehumidified by the glass cover to be T_{f2} and P_{f2}. Based on the assumptions, the heat flow of phase change can be obtained by,

$$q_{e(w\_g)} = h_{LV}\dot{m}_v \tag{6}$$

where h_{LV} is the enthalpy of phase change, which equals to the summation of the latent heat h_{fg} and the sensible heat [30].

$$h_{LV} = h_{fg} + Cp_w(T_w - T_{amb}) \tag{7}$$

$$h_{fg} = 1.91846 \times 10^6 \left[\frac{T_w}{T_w - 33.91}\right]^2 \tag{8}$$

where Cp_w is the thermal capacity of the moist air at T_w. T_{amb} is the temperature of the ambient.

$\dot{m}_v$ is the productivity of the fresh water in SS, which is related to the mass flow rate of the dry air $\dot{m}_a$ and the moisture content d,

$$\dot{m}_v = \dot{m}_a(d_w - d_g) \tag{9}$$

where d_w and d_g are the moisture content of the air at T_w and T_g, respectively, which can be calculated based on the vapor pressure P_v,

$$d = \frac{R_{g,a}}{R_{g,v}}\frac{P_v}{P - P_v} \tag{10}$$

where $R_{g,a} = 287J/(Kg{\bullet}K)$ and $R_{g,v} = 461J/(Kg{\bullet}K)$ are the gas constant of dry air and water vapor, respectively. P is the total pressure of the moist air, which is regarded as 101 kPa in the model. The vapor pressure P_v can be obtained according to the vapor temperature T_v and the relative humidity $\varnothing$ [26],

$$P_v = \varnothing e^{\left(25.317 - \frac{5144}{T_v}\right)} \tag{11}$$

$\dot{m}_a$ is related to the total mass flow rate of the moist air $\dot{m}_{mix}$,

$$\dot{m}_a = \frac{\dot{m}_{mix}}{(1 + d_w)} \tag{12}$$

where $\dot{m}_{mix}$ is decided by the air circulation velocity V and the moist air density ρ_{mix}. Based on the assumption e, the stream profile of the up-flow and down-flow air are symmetric, which indicates that half of the cross-section is occupied by the hot air that flows upward, and the other half is occupied by the cold air that flows downward. Therefore, the air mass flow rate per unit area, $\dot{m}_{mix}$, is.

$$\dot{m}_{mix} = \frac{1}{2}V\rho_{mix} \tag{13}$$

The density ρ and the heat capacity Cp of the saturated moist air at temperature t (in Celsius degree) can be obtained by the following equations and coefficients in Table 1 [31],

$$\rho_{mix,t} = \mathrm{SD}_0 + \mathrm{SD}_1 t + \mathrm{SD}_2 t^2 + \mathrm{SD}_3 t^3 \tag{14}$$

$$Cp_{mix,t} = \mathrm{SC}_0 + \mathrm{SC}_1 t + \mathrm{SC}_2 t^2 + \mathrm{SC}_3 t^3 + \mathrm{SC}_4 t^4 + \mathrm{SC}_5 t^5 \tag{15}$$

where SD and SC are the constant coefficients in Table 1.

The convective heat flow rate $q_{c(w\_g)}$ can be calculated by,

$$q_{c(w\_g)} = \dot{m}_{mix} Cp_w (T_w - T_g) \tag{16}$$

The irradiation heat flow rate $q_{r(w\_g)}$ is,

Table 1
List of coefficients for calculating the thermos-physical property of the saturated moist air (0 – 100 °C).

Subscripts	0	1	2	3	4	5
SD	1.293	−5.538E-3	3.860E-5	−5.254E-7	–	–
SC	1.005	2.051E-3	−1.632E-4	6.212E-6	−8.83E-8	5.071E-10

$$q_{r(w\_g)} = \varepsilon_1 \sigma (T_w{}^4 - T_g{}^4) \tag{17}$$

where $\sigma = 5.67 \times 10^{-8} \mathrm{W/(m^2 \cdot K^4)}$ is the Stefan-Boltzmann constant, ε_1 is the emissivity between the water and glass,

$$\varepsilon_1 = \left[\frac{1}{\varepsilon_w} + \frac{1}{\varepsilon_g} - 1\right]^{-1} \tag{18}$$

where ε_w and ε_g are the emissivity of the water and glass, respectively.

The energy conservation on the glass cover is,

$$q_{r(w\_g)} + q_{e(w\_g)} + q_{c(w\_g)} = \gamma q_{r(g\_a)} + \gamma q_{c(g\_a)} \tag{19}$$

where γ is the ratio between the glass cover area A_g and water area A_w,

$$\gamma = \frac{A_g}{A_w} \tag{20}$$

The convective heat transfer rate between the glass cover and the ambient $q_{c(g\_a)}$ is,

$$q_{c(g\_a)} = h_a (T_g - T_{amb}) \tag{21}$$

where h_a is the convective heat transfer coefficient of the ambient air.

The radiative heat transfer rate between the glass cover and the ambient $q_{r(g\_a)}$ is,

$$q_{r(g\_a)} = \varepsilon_2 \sigma (T_g{}^4 - T_{amb}{}^4) \tag{22}$$

where ε_2 is the emissivity between the glass and the ambient.

The convective heat transfer coefficient h_{h2} and the mass transfer coefficient h_{m2} of the air circulation in SS are,

$$h_{h2} = \frac{q_{c(w\_g)}}{T_w - T_g} \tag{23}$$

Therefore, h_{h2} can be rewritten as.

$$h_{h2} = \dot{m}_{mix} C p_w \tag{24}$$

$$h_{m2} = \frac{\dot{m}_v}{\rho_{v,w} - \rho_{v,g}} \tag{25}$$

The vapor density ρ_v is also decided by the vapor temperature T_v as,

$$\rho_v = \frac{P_v}{R_{g,v} T_v} \tag{26}$$

By combining equations (4), 6, 9, 12, and 13, the efficiency η_s can be rewritten as,

$$\eta_s = \frac{h_{LV} V_{mix} \rho_{mix}}{2(I + P_F)} \frac{(d_w - d_g)}{(1 + d_w)} \tag{27}$$

Thus, the heat and mass transfer coefficients, water and glass temperatures, as well as energy efficiency can be obtained by solving the above equations with the Matlab R2017a, MathWorks.Inc.

2.2. Experimental setup and devices

The photo of the indoor setup is shown in Fig. 2a. Firstly, a pyramid SS with the size of 25 cm × 25 cm is fabricated. A heating panel is placed under the basin for heating the basin and water as shown in Fig. 2b. 5 mm thickness of water is placed in the basin to be treated. The power of the heating panel is controlled by a power supply. The basin of the SS is insulated by 4 cm thickness of XPS (extruded polystyrene) foam, and the angle of the glass cover is fixed at 30°.

A thermostat cover is placed above the glass cover to simulate and control the ambient temperature. The air gap between the glass cover and the thermostat cover is 1 cm. The temperature of the thermostat cover is controlled by circulating the water from a thermostat water bath. The validation of the thermostat cover is shown in Supporting Information Note S1. The freshwater is collected by a beaker on the electronic balance. The temperatures are measured by K type of thermal couples and the temperature data is collected by a data acquisition unit. The installation detail of thermal couples is shown in Fig. S2a. All the specifications of the devices and sensors are listed in Table 2.

A fan with a diameter of 5 cm is installed inside of the SS for enhancing the inner air circulation velocity (Fig. 2b). The fan is 1 cm above the center point of the water surface. To simulate different air

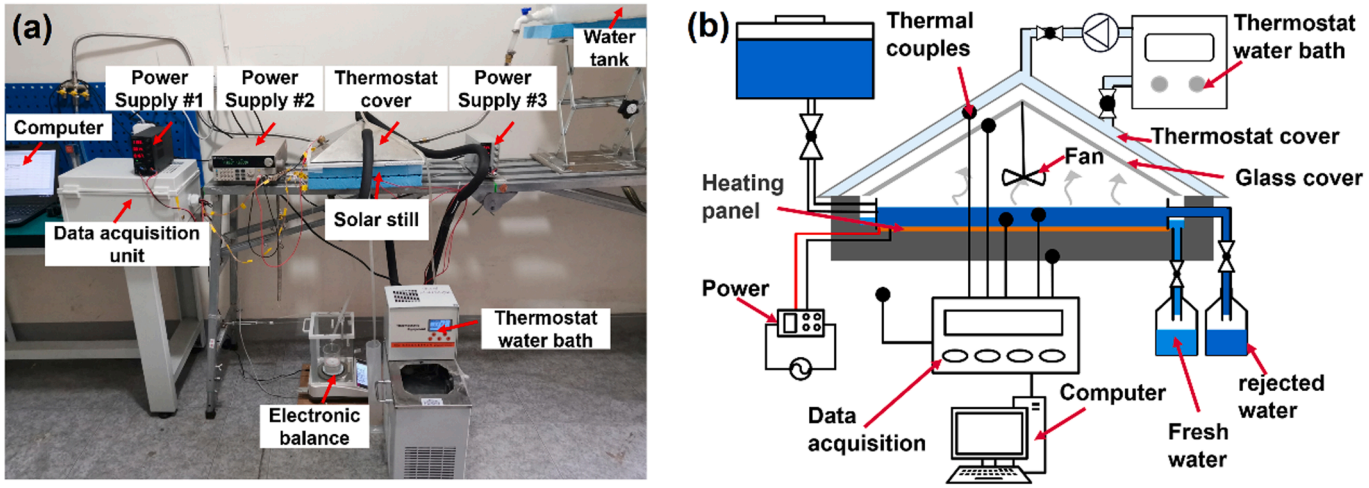

Fig. 2. (a) Photo and (b) schematic diagram of the experimental setup.

Table 2
Specific of devices and sensors in the experiments.

Name	Brand	Type	Function	Range	Error
Fan	LFFAN	LFS0512SL	Enhancing air circulation	0 ~ 4800 RPM	10% RPM
Electronic balance	ANHENG	AH-A503	Measuring productivity	0 ~ 500 g	± 0.01 g
Power supply #1 & #3	WANPTEK	NPS3010W	Supplying power for the data acquisition unit and heating panel	0 ~ 30 V	± 0.1 %
Power supply #2	ITECH	IT6932A	Supplying power for the fan	0 ~ 60 V	± 0.03 %
Data acquisition unit	CAMPBELL SCIENTIFIC	CR1000X	Collecting and saving data	–	± 0.01 °C
Thermal couple multiplexer	CAMPBELL SCIENTIFIC	AM25T	Transmitting temperature data	0 ~ 25 Channels	–
Thermostat water bath	QIWEI	DHC-2005-A	Controlling the ambient temperature around the glass cover	−20 ~ 99.9 °C	± 0.2 °C
Heating panel	BEISITE	Custom-made	Heating the water	0 ~ 2000 W/m^2	–
Thermal couple	ETA	T-K-36-SLE	Measuring the temperature	−200 ~ 260 °C	± 1.1 °C

circulation velocities, a power supply is used to control the power of the fan. The nominal voltage, current, rotation speed, and air volume of the fan are 12 V, 0.1 A, 4800 RPM (Revolutions Per Minute), and 10.5 CFM (Cubic Feet Per Minute), respectively. The mass of the freshwater was measured by the electronic balance every 10 s. The temperature data were also collected and saved by the data acquisition unit every 10 s.

The error of the experimental energy efficiency, S_η, in each experiment is propagated from the uncertainty of the measured parameters. Based on Eq. (4) and (6), S_η is determined by the uncertainty of the productivity $\dot{m}_v$, the input energy in the basin I, and the power of the fan P_F as:

$$S_\eta = \sqrt{\left(\frac{\partial \eta}{\partial \dot{m}}\right)^2 S_{\dot{m}_v}{}^2 + \left(\frac{\partial \eta}{\partial I}\right)^2 S_I{}^2 + \left(\frac{\partial \eta}{\partial P_F}\right)^2 S_{P_F}{}^2} \tag{28}$$

3. Results and discussion

The theoretical results of SS under different input power densities are shown in Fig. 3. The efficiency increases dramatically before the air circulation velocity reaches 0.02 m/s, then converges (Fig. 3a). Besides, both the heat flow rates of phase change and convection increase with the increases of air velocity at first (Fig. 3b). However, the convective heat flow rate remains lower than 40 W/m^2, which is 10 times lower than the heat flow by phase change. Therefore, the enhancement is

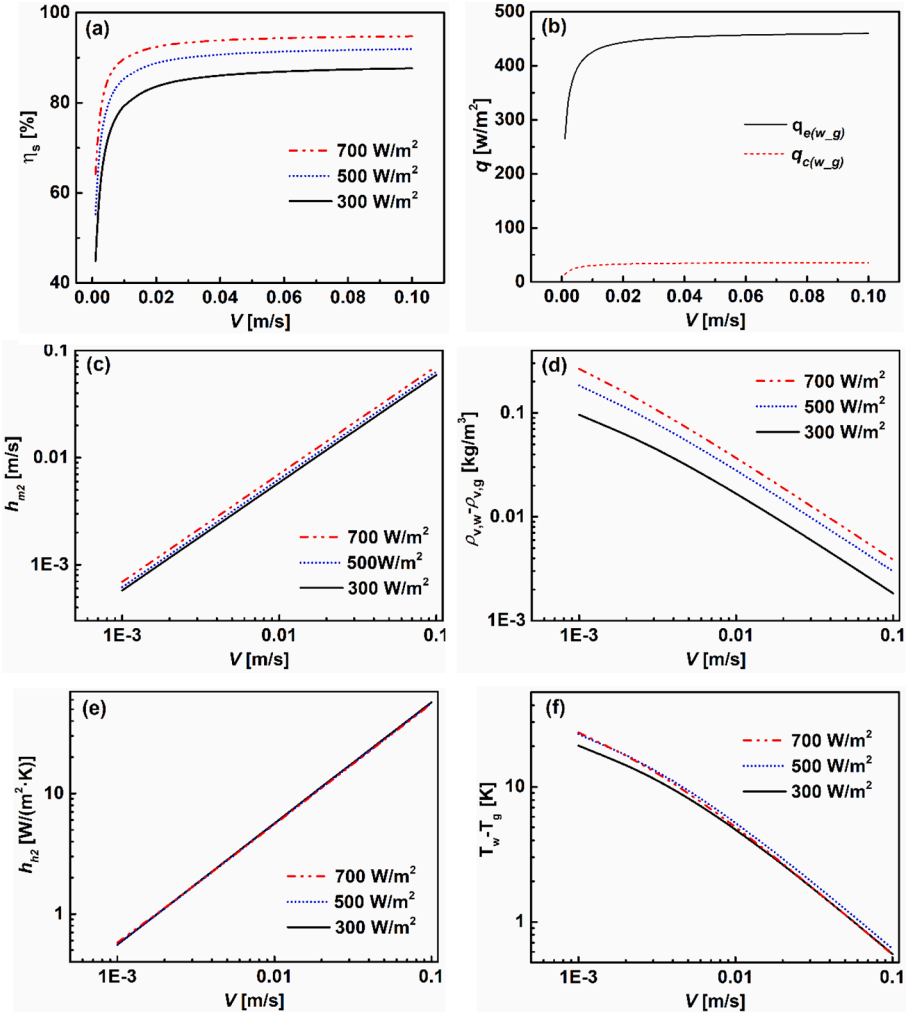

Fig. 3. Theoretical results under different input power densities, T_{amb}, h_a, and γ are fixed at 30 °C, 10 W/(m^2·K), and 1.15, respectively. (a) The theoretical efficiency of SS under different input power densities. (b) The heat flow rate of phase change and convection under 500 W/m^2 of input power density. (c) The mass transfer coefficient under different air circulation velocities and input power densities. (d) The difference in vapor density between the water and the glass cover. (e) The heat transfer coefficient under different air circulation velocities. (f) The difference in temperature between the water and the glass cover.

attributed to the significant enhancement of the phase change process. It should be noted that the ideal model assumes sufficient heat and mass transfer rates at the interfaces for all the air circulation velocities. However, the heat and mass transfer rates will be insufficient in practical application. Therefore, to approach the high energy efficiency predicted by the model, the air circulation velocity will be much higher than 0.02 m/s in practical application. Meanwhile, it is also found that the difference of vapor density and temperature between the water and glass cover decreases very fast with the increase of air circulation velocity (Fig. 3d and 3f). As a result, energy efficiency converges quickly.

Besides, the maximum efficiency of SS increases with the increase of input power density. The maximum efficiency is around 87%, 91.5% and 94.5%, for input power density at 300 W/m^2, 500 W/m^2 and 700 W/m^2, respectively. This is because, on one hand, both the mass transfer coefficient and the difference of vapor density ($\rho_{v,w} - \rho_{v,g}$) increase with the input power density (Fig. 3c and 3d). On the other hand, the heat transfer coefficient and the difference of temperature (T_w - T_g) are almost the same under different input power densities (Fig. 3e and 3f). Therefore, the heat loss from the water to the glass cover by air convection and thermal radiation is nearly constant. Thus, the enhanced mass transfer rate and the constant heat loss lead to improved energy efficiency under high input power density.

The effect of the ambient convective heat transfer coefficient (h_a) is investigated as shown in Fig. 4. Herein, a typical natural convection coefficient $h_a = 10$ W/(m^2·K) is chosen as the coefficient that represents a windless ambient of SS, and higher h_a represents a windy ambient. In the ideal model, a lower h_a gives a higher efficiency (Fig. 4a). The maximum efficiency is around 91.5%, 85% and 82.5%, for h_a at 10 W/(m^2·K), 30 W/(m^2·K) and 50 W/(m^2·K), respectively. For a higher h_a, h_{m2} decreases (Fig. 4b), and the difference of vapor density between the water and the glass cover is almost the same under different h_a (Fig. 4c). Besides, $d_w - d_g$ decreases with the increases of h_a as shown in Fig. 4d. A higher difference of moist content ($d_w - d_g$) indicates more condensable vapor mass for a given mass flow rate of the moist air. Therefore, the mass transfer coefficient, productivity, and energy efficiency decrease with the increase of h_a. The results of the ideal model indicate that, for a SS with high performance, higher wind velocity may have a negative effect due to the decreased system temperature, which agrees with previous works [32–35].

Moreover, the ambient temperature also affects the performance of SS (Fig. 5). The energy efficiency decreases with the decreases of the ambient temperature as shown in Fig. 5a. The maximum efficiency is around 91.5%, 88%, and 83%, for T_{amb} at 303 K, 293 K, and 283 K, respectively. Under lower ambient temperature, although the glass cover temperature is lower and the temperature difference is higher as shown in Fig. 5d, the overall productivity is not enhanced. This is because the productivity of the SS is not directly decided by the temperature, but by the vapor density and the mass transfer coefficient. A lower ambient temperature leads to a lower mass transfer coefficient (Fig. 5b). Besides, the vapor density difference between the water and glass cover decreases with the ambient temperature at low air circulation velocity (Fig. 5c). Thereby, the over all energy efficiency declines.

Experiments are also carried out to further understand the upper limit. Firstly, the theoretical model is validated by comparing the theoretical and experimental results of the conventional SS (Supporting Information, Fig. S3). Experimental results show that the energy efficiency of SS increases significantly when the power of the fan (P_F) increases from 0 to 0.2 W (Fig. 6a). The energy efficiency of the SS without the fan is 53.4%, 64.8%, and 71.1% at 300 W/m^2, 500 W/m^2, and 700 W/m^2 of input power density, respectively. The measured energy efficiency is high, due to the indoor experiments eliminating many losses, such as the light reflections. Therefore, the indoor experiments represent the best case that the outdoor experiments can achieve. The energy efficiency increases to 59.7%, 74.7%, and 78.7% by using 0.075 W of fan power. Then, it is increased to 68.4%, 78%, and 86.2% by using 0.2 W of fan power. The trend of results agrees with the theoretical prediction. At higher P_F, the productivity and the energy efficiency converge, which also agree with the theoretical prediction. The maximum enhancement of energy efficiency is 42%, 28%, and 20% at 300 W/m^2, 500 W/m^2, and 700 W/m^2 of input power density, respectively. Meanwhile, higher input power density also enables higher energy efficiency, which agrees with the theory.

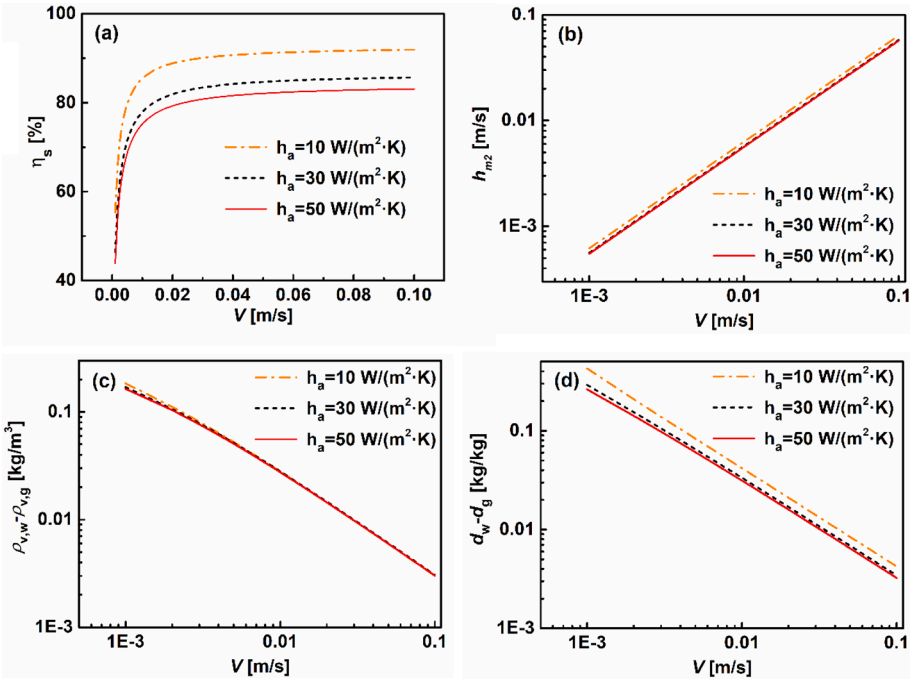

Fig. 4. Theoretical results under different ambient convective heat transfer coefficients. The input power density and the ambient temperature are fixed at 500 W/m^2 and 30 °C, respectively. (a) The energy efficiency of SS. (b) The mass transfer coefficient of inner air circulation. (c) The difference in vapor density between the water and glass cover. (d) The difference in the moist content between the water and the glass cover.

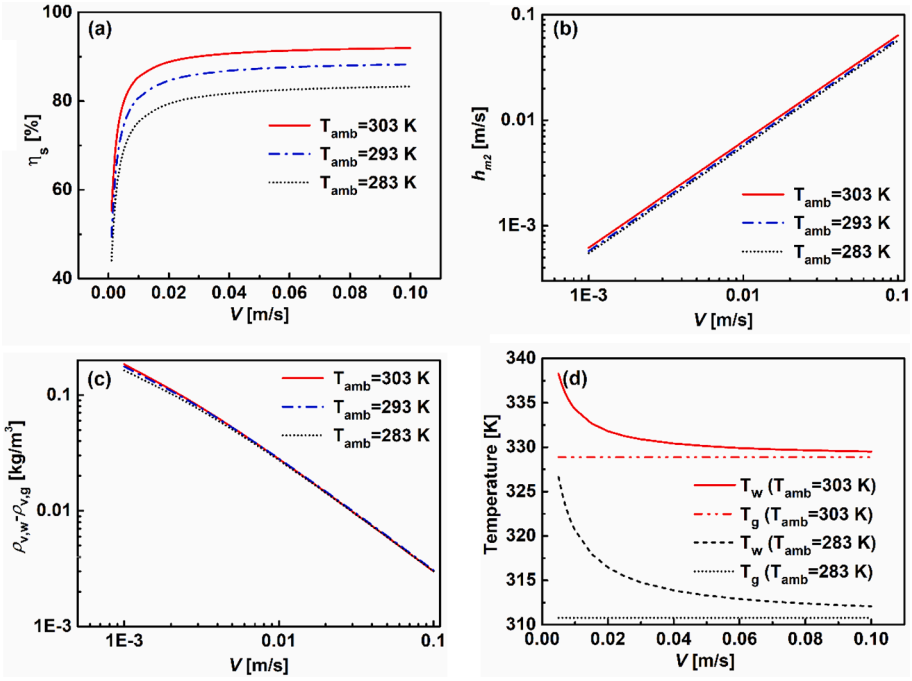

Fig. 5. Theoretical results under different ambient temperatures. I and h_a are fixed at 500 W/m^2 and 10 W/(m^2·K), respectively. (a) The energy efficiency under different ambient temperatures. (b) The mass transfer coefficient of inner air circulation. (c) The difference in vapor density between the water and the glass cover. (d) The temperature of the water and the glass cover under different ambient temperatures.

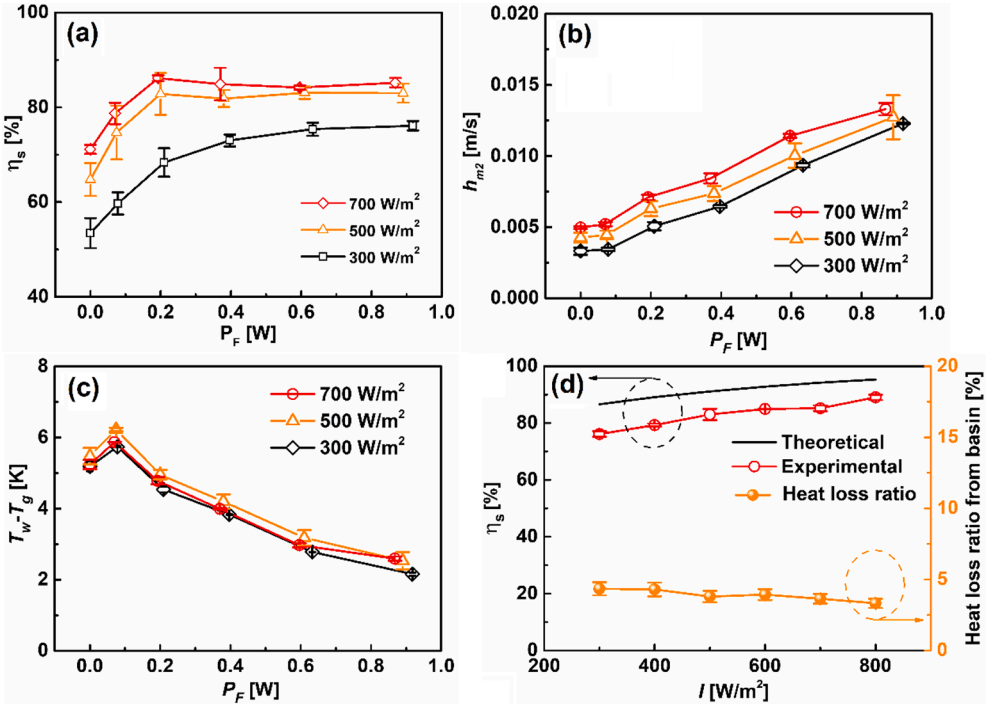

Fig. 6. Experimental results of SS under different P_F and I. The ambient temperature is fixed at 30 °C. (a) The energy efficiency of SS. (b) The mass transfer coefficient of the inner air circulation. (c) The temperature difference between the water and the glass cover. (d) maximum efficiency under different input power densities I. The ambient temperature is fixed at 30℃, h_a is fixed at 10 W/(m^2·K) for theoretical results.

The experimental mass transfer coefficients also increase with the increases of P_F. The mass transfer coefficients are lower than 0.005 m/s without the fan (Fig. 6b). The mass transfer coefficients keep increasing with P_F and reach up to>0.012 m/s when P_F is around 0.9 W. On the contrary, the temperature difference between the water and the glass cover decreases under high P_F (Fig. 6c). The enhanced efficiency indicates that the improved mass transfer coefficient compensates for the negative effect of the decreased temperature difference. Besides, it is found that the temperature difference is almost the same under different input power densities, which confirms the theoretical prediction. Nevertheless, there is a slight increase of temperature difference when increasing P_F from 0 W to 0.075 W. This might be because the fan

concentrates the hot air at the center area of the glass cover, where most of the vapor condensates. Thus the glass temperature at the side area decreases due to less heat and mass transfer as shown in Fig. S2b. As a result, the temperature difference increases at first (Supporting information Note S2).

The comparison between the maximum theoretical and experimental efficiency is shown in Fig. 6d. The maximum theoretical efficiency increases from 87% to 95.7% with the increases of the input power density from 300 W/m^2 to 800 W/m^2. As a comparison, the maximum experimental energy efficiency increases from 76% to 89%, which is 6% to 11% lower than the theoretical results. The maximum experimental efficiency is obtained by averaging the energy efficiency of $P_F > 0.6$ W. One of the main reasons for the difference is the heat loss in the experiments. Based on the temperatures of the basin and foams, it is obtained that the heat loss from the basin accounts for 3% ~ 5% of the total input power density. Given the heat loss, the experimental energy efficiencies are 3% ~ 6% lower than the theoretical efficiencies, which shows a good agreement between the theory and experiments. The experimental results under different ambient temperatures and different types of solar still also agree well with the theoretical results (Supporting Information, Fig. S4, and Fig. S5).

In addition, it is found that enhancing the inner air circulation is a cost-effective strategy to improve energy efficiency, as compared to many methods in references (Table 3). The cost of the chargeable battery and fan is only one and two dollars, respectively. The total extra cost is 3 dollars, and the power consumption is as low as 0.2 W ~ 0.6 W. Although the modification is simple, the enhancement is significant as compared to other complicated modifications in references. The high efficiency, high enhancement, as well as the economy prove the importance of improving the air circulation in SS.

This work also offers new insight into the modification of solar desalination systems with latent heat recovery, such as multistage solar still and humidification-dehumidification (HDH) systems. In multistage solar still, the first stage is affected by both solar absorption and mass transfer; the other stages are affected by the mass transfer only [38]. Economically and effectively enhancing the mass transfer to the upper limit has a dramatic effect on the utilization of latent heat, which will improve the overall performance significantly.

Besides, in the HDH system, it is common practice to control the humidity and temperature of the circulated air by using complicated structures such as corrugated surfaces or coils[39]. However, this work points out that the mass transfer upper limit may be approached by slightly enhancing the air circulation velocity in a closed chamber, without the need for structural modifications. Therefore, enhancing the air circulation velocity in a closed chamber would be a new direction of design and modification of the HDH system.

4. Conclusion

Here, the upper limit performance of solar still is analyzed based on heat and mass conservation without involving any empirical coefficients. The upper limit is affected by various factors, such as the input power density, the inner air circulation, the ambient air convention, the ambient temperature, et al. The theoretical results show that the inner air circulation has the most significant effect on the efficiency of solar still.

The energy efficiency of mass transfer increases dramatically before the ideal air circulation velocity reaches 0.02 m/s. The maximum theoretical energy efficiency ranges from 87% to 95.7% for the input power density at 300 W/m^2 to 800 W/m^2. Besides, the upper limit of the energy efficiency decreases 8.5% when the ambient temperature decreases from 30 °C to 10 °C, and the upper limit decreases 9% when the ambient convective heat transfer coefficient increases from 10 W/(m^2·K) to 50 W/(m^2·K).

Meanwhile, the maximum experimental energy efficiency is in coincidence with the theoretical results, but 6% to 11% lower. One

Table 3
Comparison of the present work and references.

Ref.	Type of SS	Basin size	Power intensity [W/m^2]	Modification	Enhancement of efficiency	Cost of extra component [$]	Power consumption [W]
This work	Pyramid SS	0.25 m × 0.25 *m*	300	Fan	42%	3	0.6
			500		28%		0.2
			700		20%		0.2
[16]	Single slope SS	0.5 m × 0.5 *m*	150 ~ 1043	External air-cooled condenser + Vacuum pump	30%	55	Missing
[18]	Single slope SS	0.625 m × 0.8 *m*	260 ~ 950	Copper oxide (Cu_2O) nanofluid + External thermoelectric cooling	80.6%	121	Missing
[20]	Single slope SS	0.5 m × 0.5 *m*	0 ~ 900	Agitation effect + external condenser	12.2%	38	4.45
[21]	Double slope SS	1.27 m × 1.06 *m*	0 ~ 1091	Fin + Phase change material + External condenser + wick material	22.33%	25	Missing
[22]	Single slope SS	1.5 m^2	200 ~ 1100	Heat sink condenser + Forced water cooling	22%	38.7	Missing
[36]	Evaporator tank + Water Collector	Diameter 0.35 m + 0.78 m × 0.56 *m*	0 ~ 850	Radiative cooling + Phase change condenser + air condenser	28%	–	14
[37]	Single slope SS	0.3 m × 0.4 *m*	0 ~ 1240	Built-in condenser + double-layered walls	54.1%	80.4	0

important reason for the difference is the heat loss from the basin to the ambient in experiments, which accounts for 3% ~ 5% of the total input power density. Moreover, the maximum energy efficiency is reached in experiments by using only 0.6 W and 0.2 W of fan power, respectively, under 300 W/m^2 and 700 W/m^2 of input power density.

In general, this work shows that, compared to other strategies, enhancing the inner air circulation is an effective and economical way to improve the performance of solar stills. This might also inspire many other solar desalination or solar thermal systems that involve inner air circulation, such as multistage solar still and humidification-dehumidification systems.

Declaration of Competing Interest

The authors declare that they have no known competing financial interests or personal relationships that could have appeared to influence the work reported in this paper.

Acknowledgment

The work was sponsored by the National Key Research and Development Program of China (2018YFE0127800), China Postdoctoral Science Foundation (2020 M682411), Science, Technology & Innovation Funding Authority (STIFA), Egypt and China, under grant (40517), and Fundamental Research Funds for the Central Universities (2019kfyRCPY045). The authors thank the National Supercomputing Center in Tianjin (NSCC-TJ) and China Scientific Computing Grid (ScGrid) for assisting in computations.

Appendix A. Supplementary data

Supplementary data to this article can be found online at https://doi.org/10.1016/j.applthermaleng.2022.118664.

References

[1] L. Rosa, D.D. Chiarelli, M.C. Rulli, J. Dell'Angelo, P. D'Odorico, Global agricultural economic water scarcity, Science Advances, 6 (2020) eaaz6031.
[2] J. Lord, A. Thomas, N. Treat, M. Forkin, R. Bain, P. Dulac, C.H. Behroozi, T. Mamutov, J. Fongheiser, N. Kobilansky, S. Washburn, C. Truesdell, C. Lee, P. H. Schmaelzle, Global potential for harvesting drinking water from air using solar energy, Nature 598 (2021) 611–617.
[3] M. Elimelech, W.A. Phillip, The Future of Seawater Desalination: Energy, Technology, and the Environment, Science 333 (2011) 712–717.
[4] P. Tao, G. Ni, C. Song, W. Shang, J. Wu, J. Zhu, G. Chen, T. Deng, Solar-driven interfacial evaporation, Nature, Energy 3 (2018) 1031–1041.
[5] G. Peng, S.W. Sharshir, Y. Wang, M. An, D. Ma, J. Zang, A.E. Kabeel, N. Yang, Potential and challenges of improving solar still by micro/nano-particles and porous materials - A review, Journal of Cleaner Production 311 (2021), 127432.
[6] A.S. Abdullah, F.A. Essa, Z.M. Omara, Effect of different wick materials on solar still performance – a review, International Journal of Ambient Energy 42 (2021) 1055–1082.
[7] K.H. Nayi, K.V. Modi, Pyramid solar still: A comprehensive review, Renewable and Sustainable Energy Reviews 81 (2018) 136–148.
[8] V.P. Katekar, S.S. Deshmukh, A review on research trends in solar still designs for domestic and industrial applications, Journal of Cleaner Production 257 (2020), 120544.
[9] F. Zhao, X. Zhou, Y. Shi, X. Qian, M. Alexander, X. Zhao, S. Mendez, R. Yang, L. Qu, G. Yu, Highly efficient solar vapour generation via hierarchically nanostructured gels, Nature Nanotechnology 13 (2018) 489–495.
[10] S.W. Sharshir, A.M. Algazzar, K.A. Elmaadawy, A.W. Kandeal, M.R. Elkadeem, T. Arunkumar, J. Zang, N. Yang, New hydrogel materials for improving solar water evaporation, desalination and wastewater treatment: A review, Desalination 491 (2020), 114564.
[11] Y. Li, T. Gao, Z. Yang, C. Chen, W. Luo, J. Song, E. Hitz, C. Jia, Y. Zhou, B. Liu, B. Yang, L. Hu, 3D-Printed, All-in-One Evaporator for High-Efficiency Solar Steam Generation under 1 Sun Illumination, Advanced Materials 29 (2017) 1700981.
[12] B. Huo, D. Jiang, X. Cao, H. Liang, Z. Liu, C. Li, J. Liu, N-doped graphene /carbon hybrid aerogels for efficient solar steam generation, Carbon 142 (2019) 13–19.
[13] M.S. Zielinski, J.W. Choi, T. La Grange, M. Modestino, S.M. Hashemi, Y. Pu, S. Birkhold, J.A. Hubbell, D. Psaltis, Hollow Mesoporous Plasmonic Nanoshells for Enhanced Solar Vapor Generation, Nano Letters 16 (2016) 2159–2167.
[14] L. Zhou, Y. Tan, J. Wang, W. Xu, Y. Yuan, W. Cai, S. Zhu, J. Zhu, 3D self-assembly of aluminium nanoparticles for plasmon-enhanced solar desalination, Nature Photonics 10 (2016) 393–398.
[15] G. Peng, S.W. Sharshir, Z. Hu, R. Ji, J. Ma, A.E. Kabeel, H. Liu, J. Zang, N. Yang, A compact flat solar still with high performance, International Journal of Heat and Mass Transfer 179 (2021), 121657.
[16] A.G.M. Ibrahim, E.E. Allam, S.E. Elshamarka, A modified basin type solar still: Experimental performance and economic study, Energy 93 (2015) 335–342.
[17] S.W. Sharshir, G. Peng, L. Wu, F.A. Essa, A.E. Kabeel, N. Yang, The effects of flake graphite nanoparticles, phase change material, and film cooling on the solar still performance, Applied Energy 191 (2017) 358–366.
[18] S. Nazari, H. Safarzadeh, M. Bahiraei, Performance improvement of a single slope solar still by employing thermoelectric cooling channel and copper oxide nanofluid: An experimental study, Journal of Cleaner Production 208 (2019) 1041–1052.
[19] S.M. Parsa, A. Rahbar, M.H. Koleini, S. Aberoumand, M. Afrand, M. Amidpour, A renewable energy-driven thermoelectric-utilized solar still with external condenser loaded by silver/nanofluid for simultaneously water disinfection and desalination, Desalination 480 (2020), 114354.
[20] R.A. Kumar, G. Esakkimuthu, K.K. Murugavel, Performance enhancement of a single basin single slope solar still using agitation effect and external condenser, Desalination 399 (2016) 198–202.
[21] S.S. Tuly, M.S. Rahman, M.R.I. Sarker, R.A. Beg, Combined influence of fin, phase change material, wick, and external condenser on the thermal performance of a double slope solar still, Journal of Cleaner Production 287 (2021), 125458.
[22] H. Hassan, M.S. Yousef, M. Fathy, M.S. Ahmed, Impact of condenser heat transfer on energy and exergy performance of active single slope solar still under hot climate conditions, Solar Energy 204 (2020) 79–89.
[23] S.W. Sharshir, A.H. Elsheikh, Y.M. Ellakany, A.W. Kandeal, E.M.A. Edreis, R. Sathyamurthy, A.K. Thakur, M.A. Eltawil, M.H. Hamed, A.E. Kabeel, Improving the performance of solar still using different heat localization materials, Environmental Science and Pollution Research 27 (2020) 12332–12344.
[24] J. Shi, X. Luo, Z. Liu, J. Fan, Z. Luo, C. Zhao, X. Gu, H. Bao, Efficient and antifouling interfacial solar desalination guided by a transient salt capacitance model, Cell Rep. Phys. Sci. 2 (2021), 100330.
[25] S. Rastegar, H. Kargarsharifabad, N. Rahbar, M.B. Shafii, Distilled water production with combination of solar still and thermosyphon heat pipe heat exchanger coupled with indirect water bath heater – Experimental study and thermoeconomic analysis, Applied Thermal Engineering 176 (2020), 115437.
[26] C. Elango, N. Gunasekaran, K. Sampathkumar, Thermal models of solar still—A comprehensive review, Renewable and Sustainable Energy Reviews 47 (2015) 856–911.
[27] Zheng Hongfei, Z.J. Zhang Xiaoyan, W. Yuyuan, A group of improved heat and mass transfer correlations in solar stills, Energy Conversion and Management, 43 (2002) 2469–2478.
[28] P.T. Tsilingiris, The influence of binary mixture thermophysical properties in the analysis of heat and mass transfer processes in solar distillation systems, Solar Energy 81 (2007) 1482–1491.
[29] D. Villanueva, A. Feijóo, Wind power distributions: A review of their applications, Renewable and Sustainable Energy Reviews 14 (2010) 1490–1495.
[30] G. Peng, S. Deng, S.W. Sharshir, D. Ma, A.E. Kabeel, N. Yang, High efficient solar evaporation by airing multifunctional textile, International Journal of Heat and Mass Transfer 147 (2020), 118866.
[31] P.T. Tsilingiris, Review and critical comparative evaluation of moist air thermophysical properties at the temperature range between 0 and 100 °C for Engineering Calculations, Renewable and Sustainable Energy Reviews 83 (2018) 50–63.
[32] J.A. Clark, The steady-state performance of a solar still, Solar Energy 44 (1990) 43–49.
[33] J.A. Esfahani, N. Rahbar, M. Lavvaf, Utilization of thermoelectric cooling in a portable active solar still — An experimental study on winter days, Desalination 269 (2011) 198–205.
[34] A.J.N. Khalifa, M.A. Ali, Indoor tests on the effect of wind speed on still performance, International Journal of Energy and Environment 6 (2015) 299.
[35] A. Rahmani, A. Boutriaa, Numerical and experimental study of a passive solar still integrated with an external condenser, International Journal of Hydrogen Energy 42 (2017) 29047–29055.
[36] A. Amarloo, M.B. Shafii, Enhanced solar still condensation by using a radiative cooling system and phase change material, Desalination 467 (2019) 43–50.
[37] P. Khalilmoghadam, A. Rajabi-Ghahnavieh, M.B. Shafii, A novel energy storage system for latent heat recovery in solar still using phase change material and pulsating heat pipe, Renewable Energy 163 (2021) 2115–2127.
[38] O. Bait, M. Si–Ameur, Numerical investigation of a multi-stage solar still under Batna climatic conditions: Effect of radiation term on mass and heat energy balances, Energy, 98 (2016) 308-323.
[39] M.H. Hamed, A.E. Kabeel, Z.M. Omara, S.W. Sharshir, Mathematical and experimental investigation of a solar humidification–dehumidification desalination unit, Desalination 358 (2015) 9–17.